EFFECT OF COPPER OXIDE ON DIELECTRIC AND MAGNETIC PROPERTIES OF SUBSTITUTED Sr-M HEXAFERRITE

A THESIS IN THE PARTIAL FULFILLMENT OF THE REQUIREMENTS FOR THE DUAL DEGREE OF BACHELOR OF TECHNOLOGY AND MASTER OF TECHNOLOGY

By

VIKASH KUMAR

710CR1175

(Under the guidance of Prof. J. Bera)

DEPARTMENT OF CERAMIC ENGINEERING
NATIONAL INSTITUTE OF TECHNOLOGY ROURKELA
ODISHA

NATIONAL INSTITUTE OF TECHNOLOGY
ROURKELA

CERTIFICATE

This is to certify that the thesis entitled, "***Effect of Copper Oxide on Dielectric and Magnetic Properties of Substituted Sr-M Hexaferrite*"** submitted by **Mr. Vikash Kumar (710CR1175)** in partial fulfilment for the requirements of the award of ***Batchelor of Technology and Master of Technology, Dual Degree*** in ***Ceramic Engineering*** at ***National Institute of Technology, Rourkela*** is an authentic work carried out by him under my supervision and guidance.

To the best of my knowledge, the matter embodied in this thesis has not been submitted to any other University/Institute for the award of any Degree or Diploma.

Date:

Dr. Japes Bera
Associate Professor
Department of Ceramic Engineering
National Institute of Technology
Rourkela-769008, Odisha

ACKNOWLEDGEMENT

I take this opportunity to express my gratitude to everyone who made it possible for me to complete my thesis successfully.

I am deeply indebted to Dr. Japes Bera, my supervisor and the guiding force behind this project. I would like to thank him for giving me the opportunity to work under him. In spite of his extremely busy schedules in SAC, he was always available to share with me his deep insights, wide knowledge and extensive experience.

I am thankful to all other faculty members of the Department of Ceramic Engineering for extending their valuable suggestions and help whenever I approached. I would also take this opportunity to express my gratitude to the non- teaching staff especially Mr. Arvind Kumar for their help and kind support. I am thankful to all my friends for having been so supportive and motivating me throughout my project.

I am also thankful to Ms. Geetanjali Parida, Mr. Ashley Thomas, Mr. Vinay Kumar R and all the research scholars in the Department of Ceramic Engineering for their kind help and providing all joyful environments throughout this work.

Last but not the least, I express my regards and obligation to my parents who taught me the values to run through all odds of life with hope and hard work.

I am sure that all that I have gained and learnt in course of this project would be of immense help to me in the future, both personally and professionally.

Vikash Kumar

710CR1175

Chapter 1

Introduction

Introduction

In recent decades, there is a constant demand for signal processing devices in mobile communication, radar, satellite, security and defense, aerospace and automotive. Moreover, the operating frequencies of these devices are constantly shifting to higher values from microwave (0.3 to 100 GHz) to millimeter wave, which requires the use of high frequency material hexagonal ferrite [1].

The group of ferrites having hexagonal crystal structures is called hexagonal ferrite or hexa-ferrite. There are numbers of hexa-ferrite compound in the general composition BaO-MeO-Fe_2O_3, where Me is a small 2+ ion such as cobalt, nickel or zinc, and Ba can be substituted by Sr. Important types of hexa-ferrites are designated as M, W, Y, Z, X and U types. The chemical formulas of them are:

- M-type: $BaFe_{12}O_{19}$ (BaM) or $SrFe_{12}O_{19}$ (SrM),
- W-type: $BaMe_2Fe_{16}O_{27}$,
- Y-type: $Ba_2Me_2Fe_{12}O_{22}$,
- Z-type: $Ba_3Me_2Fe_{24}O_{41}$,
- X-type: $Ba_2Me_2Fe_{28}O_{46}$
- U-type: $Ba_4Me_2Fe_{36}O_{60}$.

They are all ferrimagnetic materials and their magnetic properties are intrinsically linked to their crystal structure. All have magneto-crystalline anisotropy (MCA) that is the induced magnetisation has a preferred orientation within the crystal structure. On the basis of MCA, they can be divided into two main groups, those with

(1) Easy axis of magnetisation, the **uniaxial** hexaferrites and

(2) Easy plane (or cone) of magnetisation, known as **hexaplana** ferrites.

M, Z, W, X and U-types ferrites are uniaxial and Y-type is hexaplana ferrites. However, Co_2Z, Co_2W, Co_2X and Co_2U ferrites have planar anisotropy [2].

The compound with greatest technological interest is M-hexagonal ferrites. They are magnetically very hard materials due to their uniaxial and high MCA constants. Their magnetisation is locked rigidly along the preferred *c*-axis of the hexagonal structure. The high MCA is prerequisite for a high coercivity, which results a magnetically hard material suitable for permanent magnets [1]. On the other hand, hexaplana ferrites have a preferred direction of magnetization either in the hexagonal basal plane or in a cone and they are excellent soft magnet due to free rotation of magnetisation in the plane/cone. It has been reported that ferrites with planar MCA exhibit good magnetic performance in the GHz range and have higher resonance frequency compared to spinel ferrites [1]. To make them more useful in high frequency GHz application, M-ferrites are substituted with different cations (for example, Co^{2+} and Ti^{4+} for Fe^{3+}), which changes its MCA from uniaxial to planar type.

For high frequency application, the MW dielectric losses of ferrites must be minimized. The dielectric losses due to the damping of the vibration of electrical dipoles, dominate at higher frequencies, causing a high decrease of permittivity in most materials. For that reason, ferrites must have good electrical insulation and moderate permittivity to allow the full penetration of electrical field. Most hexagonal ferrites are better than cubic spinel ferrite with respect to above two properties and therefore are well suited for high frequency applications.

In addition to the high operating frequency, current generation electronic devices are becoming smaller with less weight and more efficient day by day. For that, the passive components are used in the form of multilayer chip component and are surface mounted on printed circuit boards. The recent trend is the integration of different passive components onto a single Si-wafer platform enabling more reduction of device volume and weight. For both the technologies, low temperature co-fired ceramics (LTCC) is required for co-sintering with internal metal electrode. One of such component is multilayer ferrite chip inductor (MLFCI) shown in Fig.1.

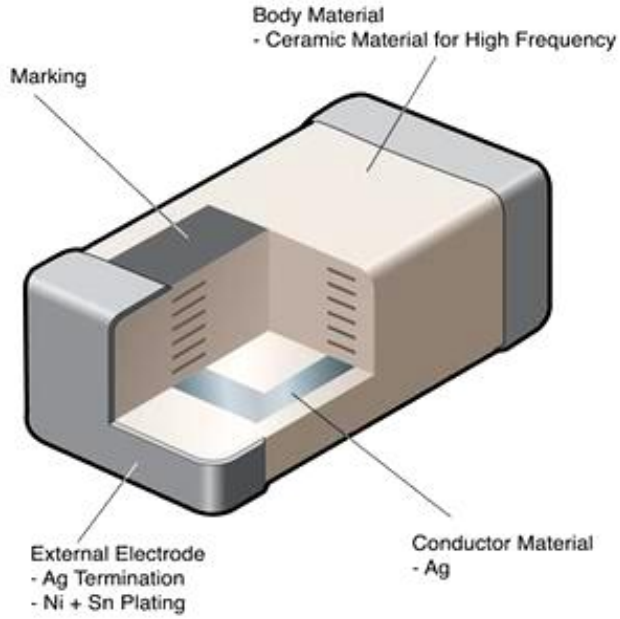

Fig. 1. Multilayer ferrite chip inductor.

Many of the MLFCI are made of soft ferrite materials like nickel-copper-zinc ferrite, with their operating frequencies in lower MHz range (Fig. 2(a)). NiCuZn ferrite is not suitable at MW/GHz frequency due to low self-resonance frequency (SRF). The SRF is the frequency above which μ_{eff} falls very rapidly due to spin relaxation, domain wall resonance, etc. SRF is defined as the

point at which μ'' is maximum and that also coincides with the half value of μ' peak. The SRF (f_r) is inversely proportional to the initial permeability (μ_i) as per the relation;

$$f_r = (0.1\gamma M_s)/\mu_i \qquad (1.1)$$

where, γ is the ratio of the magnetic moment to torque for an electron, called gyro-magnetic ratio, M_s is the saturation magnetization.

NiCuZn ferrite has SRF in the range of few MHz (~1-3) due to its high initial permeability (~900). Most hexaferrites do not have this frequency limitation as they have SRF in GHz range due to low permeability (~20). For example, $BaFe_{9.6}Co_{1.2}Ti_{1.2}O_{19}$ ferrite has SRF of 1.2 GHz [6]. The SRF (f_r) also related to the anisotropy;

$$f_r = (\gamma/2\pi)\, H_a \qquad (1.2)$$

where, H_a is the magnetic anisotropy field, which express the degree of MCA. Ba-M ferrite has high $H_a$value of 17000 Oe [2] compared to low value 198 Oe for NiCuZn ferrite [1]. This high anisotropy field produces a GHz range SRF for BaM-ferrites. In fact, Ba-M-hexaferrite has been proposed for high frequency chip application in a recent US patent [5]. SrM ferrite can be another material for high frequency application as it has slightly better magnetic properties than those of BaM [2] as shown in Table 1.

Table 1.Comparison of magnetic properties of BaM and SrM ferrites [2].M_s is saturation magnetization, H_a is magnetic anisotropy field, K_1 is magnetic anisotropy constants, and T_c is Curie temperature.

Ferrite	Formula	M_s (A m^2 kg^{-1})	H_a (kA m^{-1})	K_1 (erg/cm^3)	T_c (^{0}C)
BaM	$BaFe_{12}O_{19}$	72	1353	$3.3x10^6$	450
SrM	$SrFe_{12}O_{19}$	92-74	1592	$3.5x10^6$	460

For the fabrication of MLFCI, ferrite is co-sintered with an internal metal. Silver (Ag) is usually most suitable internal electrode as it has;

- High conductivity
- Lower cost
- Lower electrical losses.

As silver melts at 961^{o} C, the ferrite composition must be co-sintered at a temperature sufficiently lower than that, preferably at 900^{o} C, to prevent possible diffusion of Ag into the ferrite. Otherwise the diffusion of Ag metal may decrease the permeability of the ferrite. For low temperature sintering of the ferrites, usually sintering additives like glass, Bi_2O_3, are used. However, the sintering additive decreases the permeability of ferrite, and the quantity of additive should be as low as possible. Additionally, sinter-active fine ferrite powders are used for chip fabrication. Another solution could be a suitable modification of the ferrite composition enabling its low temperature sintering. As mentioned above, a recent patent [5] discloses such a modified composition of BaM ferrite which is capable of being sintered at 920^{o} C without the use of any sintering additive.

Substituted Z and Y-type hexaplana ferrites are also used for GHz applications. However, they are not so compatible with the LTCC multilayer technology. Their synthesis requires high temperatures which contradicts the required low-temperature sintering behaviour of MLFCI [7]. CoZnCu-Z and CoZnCu-Y ferrites were suggested as promising high frequency materials [8, 9]. However, they were sintered at 1300^{o} C for Z ferrite and $1000\text{-}1100^{o}$ C for Y ferrites. Nevertheless, the synthesis of single phase and thermally stable Z and Y ferrites are very difficult. Substituted Y-ferrites are thermodynamically not stable below 950^{o} C [10] and Z-

ferrites frequently decompose to a mixture of Z-, Y-, and M-type ferrites during sintering even at 900^{o} C [11]. On the contrary, Co/Ti substituted BaM ferrites are reported to be thermally stable during co-firing at 900^{o} C and have been proposed as an excellent magnetic material for MLFCI [7]. In this case, a low temperature glass sintering aid was used to produce a dense ferrite with a permeability of μ'=13 and SRF of 1 GHz.

With this background, it may be concluded that SrM ferrite will be a good candidate for high frequency chip application with respect to the enhancement of SRF. As stated above, SrM ferrite has higher saturation magnetization and magnetic anisotropy field H_a than BaM ferrite and expected to show better high frequency properties compared to BaM ferrite.

Chapter 2

LITERATURE REVIEW

Literature Review

In this section an effort has been made to provide a detailed review of the research work undertaken by various researchers on the synthesis of $SrFe_{12}O_{19}$ and the effect of doping of various divalent cations on the magnetic and electric property as well as the effect of various sintering additives on the sintering temperature.

Many research works have been carried out to improve the elecro-magnetic properties of $SrFe_{12}O_{19}$. One of these attempts is by the substitution of various divalent cations like Co ,Ti , Zn, La (trivalent) in $SrFe_{12}O_{19}$.

The Sr-M ferrites have been synthesized through different routes like; conventional solid oxide reaction [12], co-precipitation [13], sol-gel [14], hydrothermal [15], glass crystallization [16], combustion method [17], etc. The phase formation of these hexaferrites is an extremely complicated process and their formation mechanisms are not yet fully understood [2]. SrM has been synthesised through conventional solid oxide reaction by calcining oxide raw materials at 1000^{o} C for 12 h [12]. However, the phase can be synthesized at a temperature as low as 700^{o} C by sol-gel processing [14]. So the sol-gel processing could be an effective route for the synthesis of fine-grained sinter-active ferrite powders.

Magnetic properties of the ferrite depend on many parameters like density, grain size, chemical composition and grain alignment. In general, higher is the density higher will be saturation magnetization (M_s) and lower the grain size higher will be coercive field (H_c). The cation substitution is one of the most important methods for improving magnetic properties of

ferrites. M_s of the ferrite can be increased by the substitution of non-magnetic Zn^{2+} for Fe^{3+}, where Zn^{2+} prefers tetrahedral positions of the crystal structure. The substitution reduces the negative contribution of tetrahedral-octahedral anti-ferromagnetic coupling. Other 2-valence cations like Cu, Ni, Co, Mg and Mn have also been substituted for Fe^{3+}. The charge compensation for these substitutions is done either by substituting Ba with 3-valence cation or by substituting Fe with 4-valence cation. Different 3-valance cations like V, Ga, Al, In or Sc and 4-valance cations like Ti, Sn, Zr, Hf, Ce or Ru have been substituted in the ferrite [2].

The most common substitution in M-ferrite is $BaCo_xTi_xFe_{12-2x}O_{19}$ and the substitution is very important for tailoring anisotropy and microwave properties of M-ferrite [2]. With the increase in *x*, grain size, M_s *and* H_c decreases. Ti plays major role in decreasing grain size and Co plays role in the change of magnetic properties. The axial anisotropy of the ferrite decreases with the substitution and converted into in-plane anisotropy. Hence, a very soft ferrite can be achieved with the substitution while keeping M_s value reasonably stable. Other major advantage of Co^{+2}/Ti^{+4} substitutions is increased resistivity of the substituted ferrite. Similar behavior is found in other substitutions like; CoZr-*M*, CoSn-*M*, NiZnTi-*M*.

It has been found that a stoichiometric mixture of ferrite powders never sinter fully, whereas Fe deficient material can be fully densified. This is attributed to increased diffusion rates in the non-stoichiometric mixes due to induced lattice defects. For co-sintering with Ag internal electrode in a MLFCI, the sintering temperature of ferrite must be reduced to 900^o C or less. Two most effective approaches to reduce the sintering temperature are (1) Use of additives like glass, Bi_2O_3, B_2O_3, SiO_2, for liquid phase sintering and (2) Partial substitution of metal cations by Cu or addition of CuO. There are only few reports on reduction of sintering temperature of Sr-M

ferrite by CuO addition [18, 19]. The major mechanism proposed [12] for enhanced sintering was the formation of Cu-rich eutectic phase which melts below 1000^{o} C and enabled the reactive liquid-phase sintering of CuO added SrM ferrite. They also proposed that Cu^{2+} was not substituted in hexagonal structure, rather spinel type Cu-ferrite and Cu-rich eutectic phases were formed.

There are very few international patents on this typical issue. The patent on "Ferrite Material for a Permanent Magnet and Method for Production There of" [18], disclosed about low temperature sintered Sr-M ferrite for MLFI application. However, one recent patent [5] discloses about the composition based on the low temperature sintered Ba-M ferrite for chip bead and antenna application in few 500 MHz frequency band. There are no Indian patents available related to this specific subjects.

Wandee Onreabroy et. al. [20] investigated the structural and magnetic properties of $Sr_{0.8}La_{0.2}Fe_{12}O_{19}$ which were fabricated by conventional ceramic process. It was observed by studying the XRD patterns that the undoped sample had a hematite phase which was much lower in case of the doped specimen. By SEM analysis it was also observed that by the doping of La^{+3} caused a lesser increase in average grain size as compared to the undoped specimen. The study also showed that the doped sample had higher values of saturation magnetization than before.

Ali Ghasemi et. al. [21] prepared Sn and Zn substituted Strontium hexa-ferrite by a sol-gel process on thermally oxidized silicon wafer (Si/SiO2). The SEM analysis of samples showed that on increasing Sn-Zn content the grain size decreased. It was also observed that by increasing the

substitution content in the ferrite thin films, the coercivity value and saturation magnetization values increased but magnetic interaction reduced.

Qingqing Fang et. al. [22] prepared strontium hexa-ferrite nanoparticles through a chemical sol-gel process. The strontium hexa-ferrite was substituted by Zn^{+2}, Ti^{+4}, Ir^{+4} and it was observed that $(Zn, Ti)_x$ shows higher values of both coercive field strength and saturation magnetization than the $(Zn, Ir)_x$ substituted phase for $0 < x \leq 0.6$.

Xiansong Liu et. al. [23] synthesized strontium hexa-ferrite by ceramic process where Sr^{+2} was substituted by La^{+3} and Fe^{+3} was substituted by Co^{+2} according to the formula $Sr_{1-x}La_xFe_{12-x}Co_xO_{19}$. It was observed that when an appropriate amount of substitution of La^{+3} and Co^{+2} was done then an increase in saturation magnetisation and intrinsic coercivity resulted.

Ali Ghasemi [24] prepared $SrFe_{12-x}(Zr_{0.5}Mg_{0.5})_xO_{19}$ by sol-gel method where x = 0 to 2.5. The magnetic properties of this sample was studied with the help of a vibrating sample magnetometer (VSM) and it was observed that with an increase in Zr-Mg substitution content the coercivity decreases but saturation magnetisation value increases.

Kubo et. al. [25] invented a composite type magnetic particles (A) each of which contains hexagonal ferrite and spinel structure ferrite and single phase type magnetic particles of hexagonal ferrite (B). This type of magnetic particle has a stronger resistance to noise than that made by using single phase type magnetic particles of hexagonal ferrite thereby providing excellent electromagnetic characteristics. This also provides a higher signal to noise ratio for

short wavelength range. The formula for the compound is $AO_n(Fe_{12-x-y}M(1)_xM(2)_yO_{18-z})$ where A = Ba / Sr / Ca / Pb , M(1) = Co / Zn / Ni / Cu / Mn / Fe, M(2) = Ti / Sn / Ge / Zr / Sb / Nb / V / Ta / W / Mo. X can vary from 0.5 to 0.3 , Y from 0 to 2.0 and Z can be 0.05 or larger. When A : B = 5 : 95 to 30 : 70 it can be used as a magnetic recording medium for 1μm wavelength or lower and when A : B = 70 : 30 to 95 : 5 it can be used for 1μm wavelength or higher.

Objective:

Objective of the present work is to investigate the effect of CuO addition on the (a) phase formation, (b) phase stability, (c) Dielectric and (d) Magnetic properties of CoTi substituted Sr-M Hexagonal ferrite.

Chapter 3

EXPERIMENTAL PROCEDURES

Synthesis of Co-Ti-Strontium M-Ferrite Powder

Co-Ti-Strontium M-Ferrite Ferrite powders were prepared by sol-gel auto combustion method. AR grade Strontium Nitrate [$Sr(NO_3)_2$], Cobalt Nitrate [$Co(NO_3)_2.6H_2O$], Copper Nitrate [$Cu(NO_3)_2.6H_2O$], Iron Nitrate [$Fe(NO_3)_3.9H_2O$], Citric Acid [$C_6H_8O_7.H_2O$] were used as raw materials in auto combustion method. TiO_2 powder and Tetra-isopropyl-ortho-titanate ($C_{12}H_{28}O_4Ti$) were used as source of TiO_2 in the synthesis.

Sol-gel combustion synthesis

Pure and Co-Ti substituted $SrFe_{12}O_{19}$ (SrM) ferrite powders were synthesized by sol-gel auto combustion process. This process has advantages such as low energy consumption, simple equipment requirement, simple preparation method and soluble precursors which give homogeneous, nano-sized, highly reactive powders [26]. The auto combustion synthesis process also known as self-propagating synthesis was first developed by Merzhanov and had been used successfully in preparation of complex oxides like ferrites [27].

Sol-gel auto-combustion synthesis route involves exothermic redox reaction between organic fuel and a metal nitrate to yield multi-element oxide. The auto-combustion synthesis is self-sufficient to provide the energy required for the reaction to take place. The organic fuel along with metal nitrates is mixed with distilled water to form a solution which maximizes the molecular mixing of the constituent components. This solution is then slowly heated to dry and ultimately transform it to a gel.

The gel eventually ignites in a self-propagating combustion manner until all the gel is completely burnt out. This self-propagating combustion reaction lasts about 2-5 seconds to yield the desired

product. This route yields a highly homogeneous product in a very short period of time which does not require the usage of expensive high temperature furnaces. The parameters that influence an auto-combustion synthesis reaction are fuel to oxidizer ratio (f/o), ignition temperature, water content of the precursor mixture and the type of fuel used. The fuel to oxidizer ratio is critical from the reaction point of view. The flame temperature of the reaction can be controlled by varying ratio of fuel to oxidizer.

Fig. 2 shows the flow diagram for auto-combustion synthesis of Co-Ti Sr M-ferrite powders.

Ferrite powder was synthesized by an amount of 10 gm. per batch. Briefly to prepare 10 gm. Sr $Co_{1.3}Ti_{1.3}Fe_{9.4}O_{19}$ ferrite, 1.989 gm strontium nitrate, 3.556 gm. cobalt nitrate, 0.976 gm. titanium oxide, 35.69 gm. Iron nitrate and 59.21 gram of citric acid was mixed in to the solution.

In Co, Ti, CuO substituted $SrFe_{12}O_{19}$ as, required moles of constituents were added to the solution before the addition of citric acid. The mixture thus obtained was placed in a beaker and was homogenized by stirring. Then the pH of the solution was approximated to 7 by the addition of ammonia solution. Then the solution was heated slowly on a hot plate at a temperature of 80^{o}C. This continuous slow heating gives rise to a sol which then converts to a gel. For the synthesis of Ti substituted Sr-M ferrite Titanium dioxide was used.

The gel thus obtained was dried at 200^{o}C until the gel ignited in a self-propagating combustion manner and finally yielding a fluffy structured material. This fluffy material was further ground and again calcined at 1200^{o}C for 4 hours. Finally, calcined powder was ground to get ferrite powder.

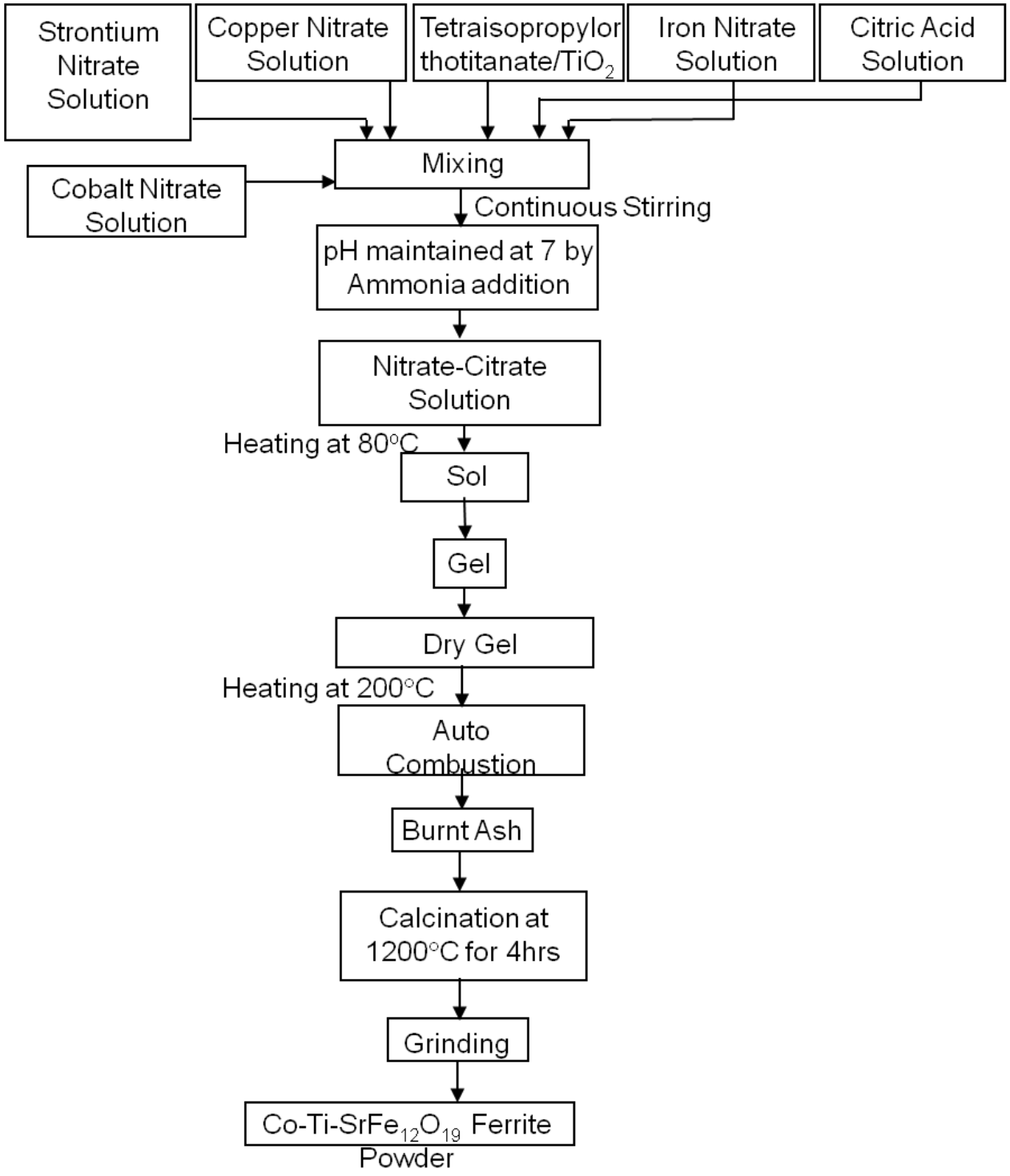

Fig. 2. Flow diagram for auto combustion synthesis of Co-Ti-$SrFe_{12}O_{19}$ ferrite powder.

Dried gel and powder characterization

Thermal Characterization

The dried gel was characterized by differential scanning calorimetry (DSC) and thermo gravimetric analysis (TGA) using NETZSCH STA (Model No 409C). This technique is excellent to get an idea about decomposition behavior, phase transitions, formation of products, etc. of precursor powders synthesized through different routes.

Exothermic or endothermic changes are shown in opposite directions of the baseline. TGA is a simple analytical technique that measures the weight loss (or weight gain) of a material as a function of temperature. As materials are heated, they can lose weight due to drying, or from chemical reactions that liberate gasses. Some materials can gain weight by reacting with the atmosphere in the testing environment.

In DSC, heat flux required to maintain the temperature of both test sample and inert sample is measured. This heat flux is measured in mW/mg./

Phase Analysis

The phase formation characteristic of the burnt and calcined ash powder was studied by using powder X-ray Diffraction performed with the help of Rigaku's Diffractometer (model-ultima 4, Japan). For the detection of diffracted X-rays, there is an electronic detector on the other side of the sample in the X-ray tube. The sample is then rotated through different Bragg's angles. The track of the angle (θ) is kept with the help of a goniometer, the detector records the detected X-rays in counts/sec and sends this data to the computer. After the complete scan of the sample the X-ray intensity versus angle theta (2θ) is plotted.

Densification study

The densification kinetics of compact rectangular samples was done with the help of NETZSCH dilatometer model DIL 402 C. In the dilatometer the sample is placed in a sample holder which is situated in the centre of the furnace. The shrinkage or expansion characteristic of the sample is recorded by a push rod (pressed against the sample inside the furnace) which is connected to the measuring head. This experiment was carried out for different samples for temperature ranges like room temperature to 1200^{o}C at a rate of 10^{o}C per minute in an atmosphere of air.

Fabrication and sintering of ferrite parts

Fabrication

The powder of each batch which was earlier calcined at 1250^{o}C for 4 hours was mixed with 5 wt% binder (polyvinyl alcohol). The following flow diagram (Fig. 3) shows the entire process. Initially the calcined powders were mixed with 5 wt% PVA binder solution for about 2 hours and then dried at about 50^{o}C. Then the resulting specimen was granulated and then pressed in the form of pellets with diameter-13mm, and thickness- < 2mm using a uniaxial hydraulic press at a pressure of 4 Tonnes for 90 seconds.

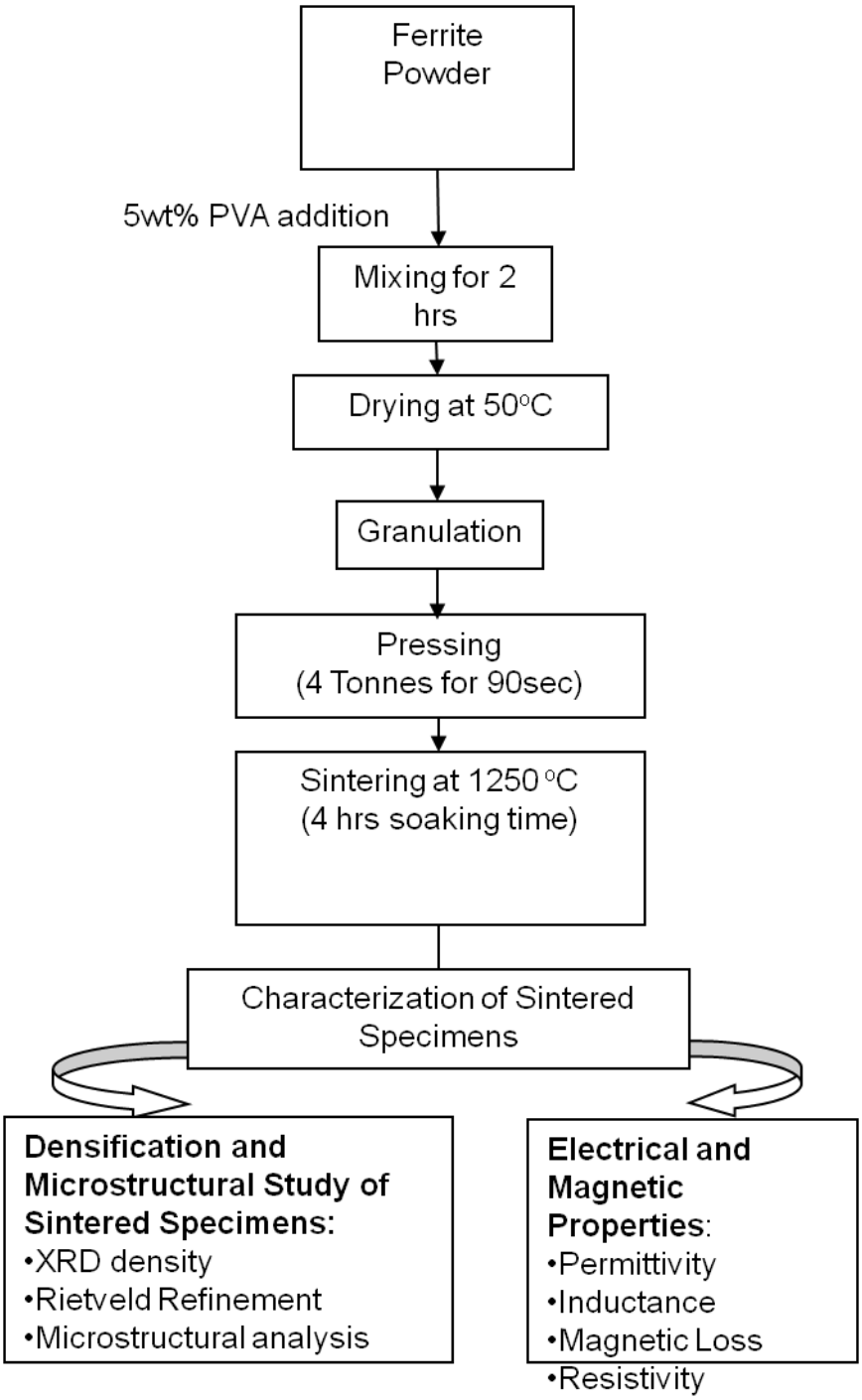

Fig. 3. A flow chart of fabrication and characterization for sintered ferrite parts.

Sintering

The uniaxially pressed pellet samples were sintered in an electric furnace at various temperatures 1200^{o}C for 4 hours. The thermal regime of the furnace was controlled through a "Eurotherm" programmer-cum-controller within ± 2°C accuracy. The pellet samples were heated from room temperature to 650^{o}C at 1^{o}C/min followed by soaking at 650^{o}C for 2 hours and then heating at 3^{o}C/min till the sintering temperature and then soaking at the sintering temperature for 4 hours. Then the samples were cooled inside the furnace at 3^{o}C/min till room temperature was reached.

Characterization of Sintered Specimens

The physical properties of the sample such as microstructural analysis and phase analysis were done. The dielectric and magnetic properties were also characterized for torroids and sintered pellet samples.

Density and Apparent Porosity

Bulk density and apparent porosity of sinter specimens were determined by Archimedes principle. Sintered samples were weighted in dry state. Samples were immersed in water and kept under a vacuum of 4 mm of mercury for 5 hrs to ensure that water filled up the open pores completely. Then, soaked and suspended weights were measured. The apparent porosity and bulk density were calculated as follows:

Dry weight of the sample = W_d, Soaked weight of the sample = W_s, Suspended weight of the sample = W_a

$$\%\,P_{App} = \frac{W_s - W_d}{W_s - W_a} X100$$

$$D_{bulk} = \frac{W_d}{W_s - W_a}$$

Microstructural Analysis

The microstructures of the sintered pellets were studied with the help of Field Emission Scanning Electron Microscopy (FESEM). The FESEM has an electron gun which under vacuum conditions emits a beam of electrons which is allowed to pass through a series of electromagnetic lenses before falling on the surface of the sample. The voltage range of the electron beam is in the range of 1-30 kV. When the electron beam interacts with the surface of the sample a part of it is reflected as back scattered electron (BSE) and also as low energy secondary electron (SE), cathode luminescence, X-ray excitation beam and some part of the electron beam is transmitted. The secondary electron beam forms an image which is studied in the extrinsic mode of SEM. These secondary electrons are then displayed on a television screen. The image thus formed would be bright if there is high secondary electron emission and this type of high emission is due to surface structure of the sample. The final picture which is obtained has brightness associated with surface characteristics and the image is normally illuminated. The samples were mounted on a metal stub with carbon paint. The mounted samples were studied by SEM (FEI).

Phase analysis:

The phase analysis was done by using XRD technique using X-Pert High-Score software. Lattice parameters were evaluated through Rietveld refinement. In Rietveld method the principal goal is to refine crystal structure. The things actually being refined are parameters in models for the crystal structure and for other specimen and instrument effects on the diffraction pattern. In this method the least squares refinements are carried out until the best fit is obtained between the entire observed powder diffraction pattern taken as a whole and the entire calculated pattern based on the simultaneously refined models for the crystal structures, diffraction optics effects,

instrumental factors and other specimen characteristics i.e. lattice parameters as may be desired and can be modelled.

Dielectric characterization

For the dielectric characterization the sintered pellet samples were first cleaned with acetone and then a layer of silver paste was applied on the top and bottom surface of each pellet. Then these pellets were cured in a furnace at 650^{o}C for 30 mins. After curing the dielectric test of these samples was carried out.

The device used for this characterization was LCR HiTESTER (Model 3532-50) HIOKI. The measurements for this test were taken in the range of 100Hz to 1MHz. The graphs of tan δ vs frequency and permittivity vs frequency were plotted and analysed, where tan δ = dissipation or loss factor and relative permittivity is:

$$\acute{\varepsilon} = \frac{C \times d}{\acute{\varepsilon} \times A}$$

ε'' = relative permittivity of air (8.854×10^{-12} F m^{-1})

C = capacitance

d = thickness of pellet

A = area of the top surface of pellet.

Inductance and Magnetic Loss

Magnetic loss and inductance are the most primary magnetic characteristic property of any ferrite. The instrument that was used to measure this property was the LCR HiTESTER (Model 3532-50) HIOKI. This instrument has a maximum frequency limit of 5 MHz and was used to measure *tan δ* and inductance on toroid samples which were wound by low capacitive six turns of enamelled copper wire. The importance of this winding is that the stray capacitance (unwanted

capacitance which can allow signals to leak between circuit wires) can be reduced by this special winding of the ferrite core.

The inductance of a ferrite core depends upon length of the coil, number of turns, diameter of the coils and the nature of the ferrite composition. Inductance is the ratio of the total magnetic flux linkage to the current (I) through the ferrite core. The total magnetic flux linkage depends on magnetic permeability (μ) of the medium or core material. This tells us that magnetic inductance is directly proportional to magnetic permeability. The initial permeability was calculated from the data of inductance by the use of the following formula:

$$\mu' = \frac{L}{2 \times 10^{-7} \times Na^2 \times H_t \times \ln\left[\frac{D_o}{D_{in}}\right]}$$

Where L = inductance

N_a = number of turns

H_t = height of toroid

D_o = outer diameter of the toroid

D_{in} = inner diameter of the toroid

Many core losses which occur in cases of ferrites are due to hysteresis loss, eddy current losses and residual losses. The generation of hysteresis loss is due to irreversible rotation of magnetization vector. The eddy current loss is generated due to the current induced in the core under the influence of a time varying magnetic flux. The residual loss is caused by the power dissipation due to the reversible domain wall damping and the reversible rotation of domains. The relative loss factor (RLF) which is the ratio of *tan δ* (loss tangent) to *μ'* (initial permeability) was calculated.

Resistivity

The sintered hexagonal ferrite pellets were coated with conductive silver paste and cured at 650^{o}C for 30 mins. The AC resistivity ρ can be calculated as per the following formula:

$$\rho = \frac{1}{\omega.\varepsilon o.k'.\tan\delta} = \frac{A}{2\Pi f.\tan\delta.C.t}$$

where, ε_0= permittivity of free space

k' = relative dielectric constant

$\tan\delta$ = dissipation or loss factor

ω = angular frequency

C = capacitance

A and t are the area and thickness of the sintered pellet respectively.

Chapter 4

RESULTS

AND

DISCUSSION

Results and Discussion

Thermal Characterization

The thermal decomposition behavior of gel was studied by differential scanning calorimeter and thermo gravimetric analysis. Fig.4 shows the DSC and TG curve of the gel precursor. The DSC curve shows two exothermic peaks at 390°C and 460°C respectively. The TGA curve exhibited two step weight losses, one in the range of 84-200°C and other in range of 280-500°C.

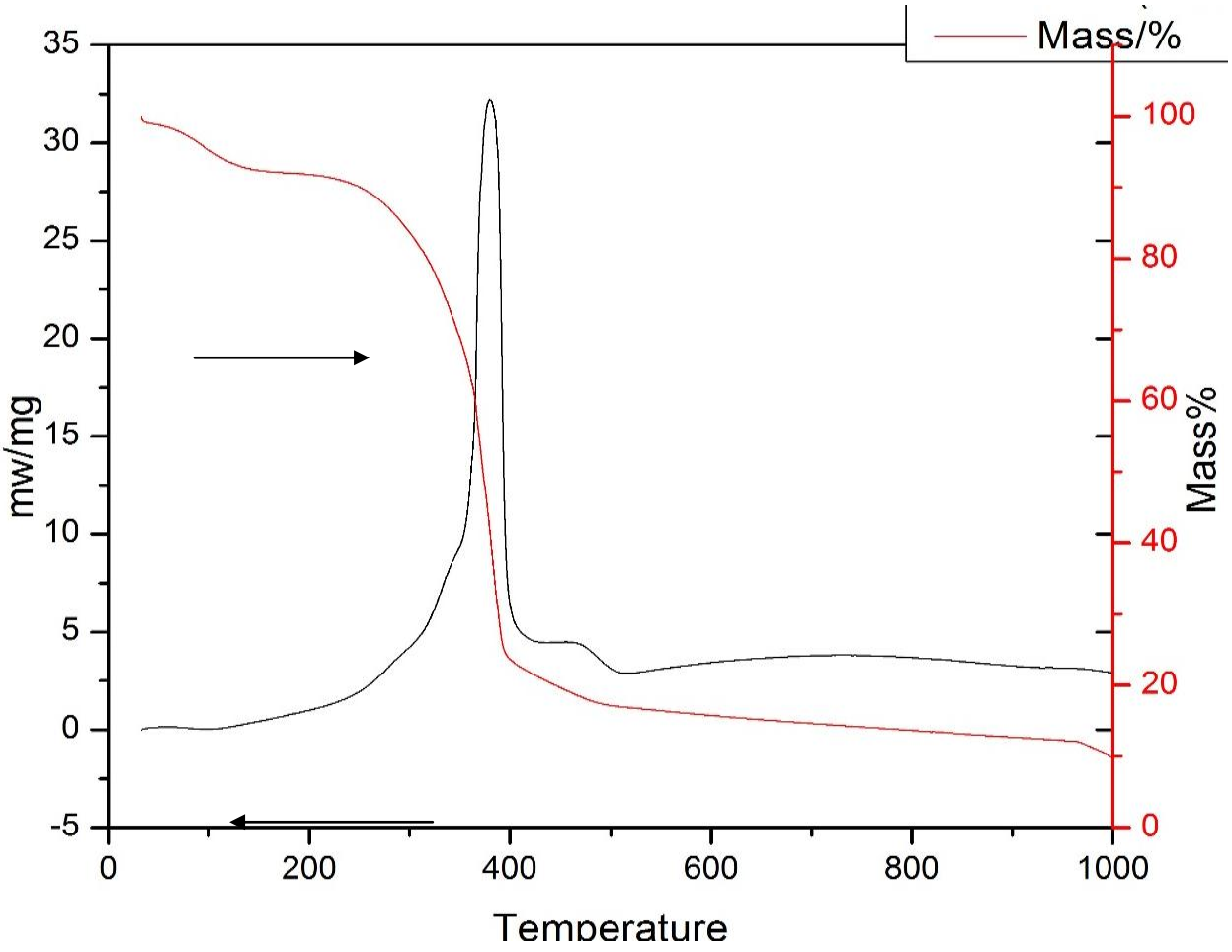

Fig. 4. DSC-TG plots for the nitrate-citrate gel with a heating rate of 10^{o}C /min in air atmosphere

The autocatalytic combustion process occurred at 390°C causing 61.4% weight loss. The small DSC peak at 460°C is due to removal of residual organic fuel. The combustion process, an exothermic one, can be considered as a thermally induced anionic redox reaction of the gel in which the carboxyl groups act as reductant and NO^{3-} ions act as oxidant. In the combustion process heat is released which supply the energy needed to react the components to form Sr-Co-Ti-ferrite through solid-state diffusion process. During combustion CO_2, N_2, and H_2O gasses are released. The nitrate-citrate combustion reaction for x= 0 composition may be stated as:

$$Sr(NO_3)_2 + 1.3Co(NO_3)_2 + 2Fe(NO_3)_3 + 3C_6H_8O_7 \longrightarrow (SrCo_{1.3}Ti_{1.3})Fe_2O_4 + 4N_2\uparrow + 18CO_2\uparrow + 12H_2O\uparrow$$

Phase Evolution:

The phase formation behavior was studied by XRD. Fig. 5 shows the XRD patterns of the as-burnt ferrite powders.

As burnt powder XRD pattern (Fig 5a) shows mostly amorphous pattern. However the crystalline TiO_2 phase diffraction peak was observed at around 25 degree 2-theta positions in the specimen. This is because in this synthesis TiO_2 powder was used which does not go in to the solution during gel formation as it is not soluble into the water.

Fig 5b shows the XRD pattern of powder calcined at 700^oC. It shows the formation of intermediate cubic $CoFe_2O_4$ ferrite and un-reacted TiO_2. Strontium based compound may be in the amorphous state. So the reaction takes place through the step:

$$CoO + Fe_2O_3 \longrightarrow CoFe_2O_4$$

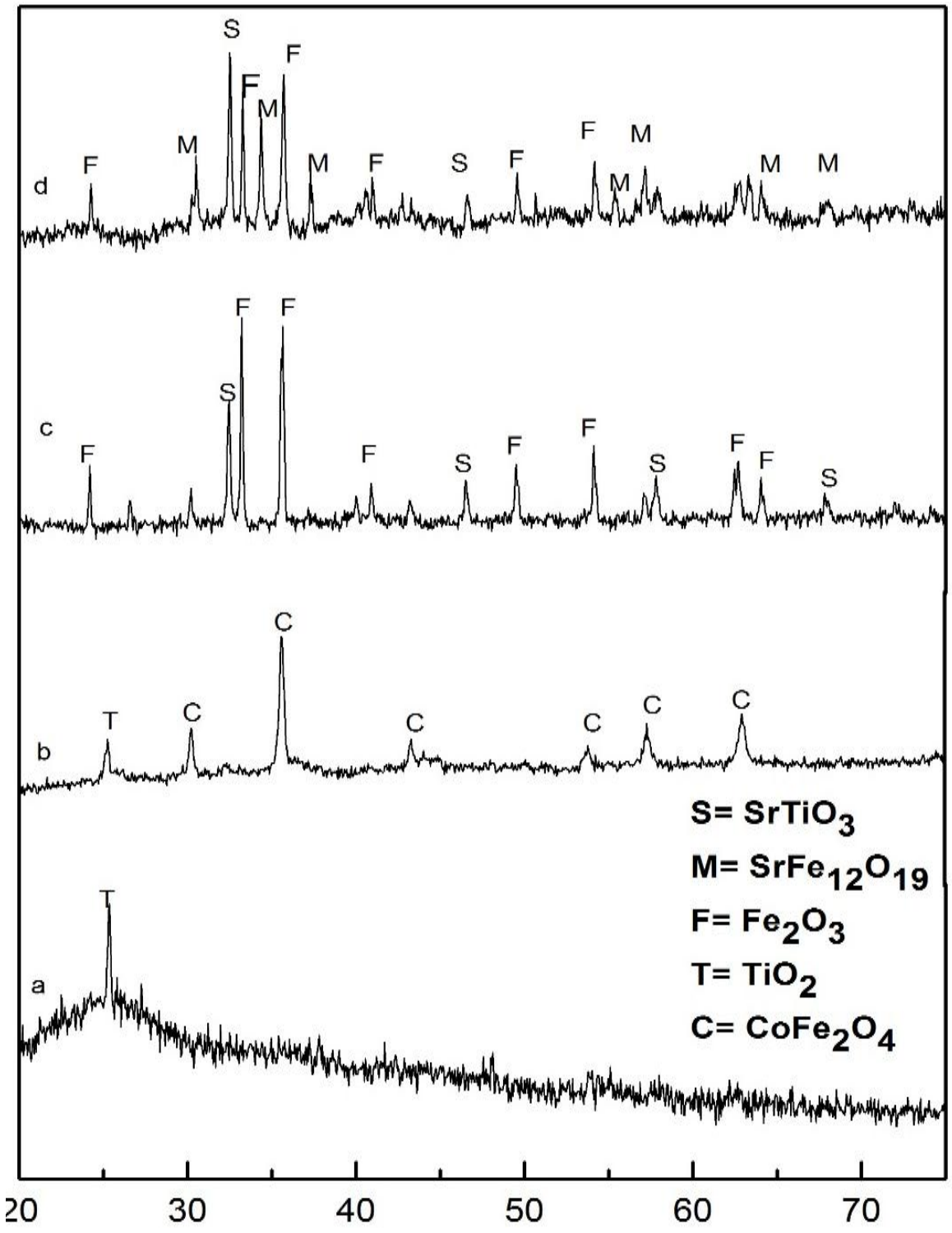

Fig. 5 Room temperature XRD pattern of Sr-M hexaferrite precursor powder calcined at (a) as burnt, (b) 700 (c) 900 and (d) 1100°C. Major phases identified are also shown in the figure.

Powders were calcined at 900°C and phase analysis of that (Fig 5c) shows that there was formation of iron oxide and strontium oxide from amorphous powder because about 60% Fe_2O_3 phase was found in the specimen. Semi-quantitative phase estimation was carried out using Philips X'pert Highscore software. Other phases present were about 25% $SrTiO_3$ and 15% $CoFe_2O_4$. The SrO was released from amorphous material, however it reacted immediately with TiO_2 to form $SrTiO_3$. The reactiom may be as follows

$$\text{Amorphous material} + TiO_2 \xrightarrow{900°C} Fe_2O_3 + SrO$$

$$SrO + TiO_2 \xrightarrow{900°C} SrTiO_3.$$

So the analysis indicates that the Sr-M ferrite phase formation require higher temperature than 900°C. The powder was next calcined at 1100°C. The XRD pattern (Fig 5d, 1100°C) shows that there was about 35% formation of Sr-M ferrite phase. The remaining intermediate phases were Fe_2O_3 ~44% and $SrTiO_3$~15%. Finally the desired phase was formed through the reaction:

$$Fe_2O_3 + SrTiO_3. + CoFe_2O_4 \longrightarrow SrCo_{1.3}Ti_{1.3}Fe_{12}O_{19}$$

So, these results indicate that the pure Sr-M ferrite phase formation require still higher temperature than 1100°C. That is why the preparation technique was changed where Ti-isopropoxide raw material was used as a source of TiO_2 in place of TiO_2 powder.

The ferrite was then synthesized using Ti-isopropoxide ($C_{12}H_{28}O_4$) as TiO_2 source through combustion route. Fig 6 shows the XRD pattern for this specimen.

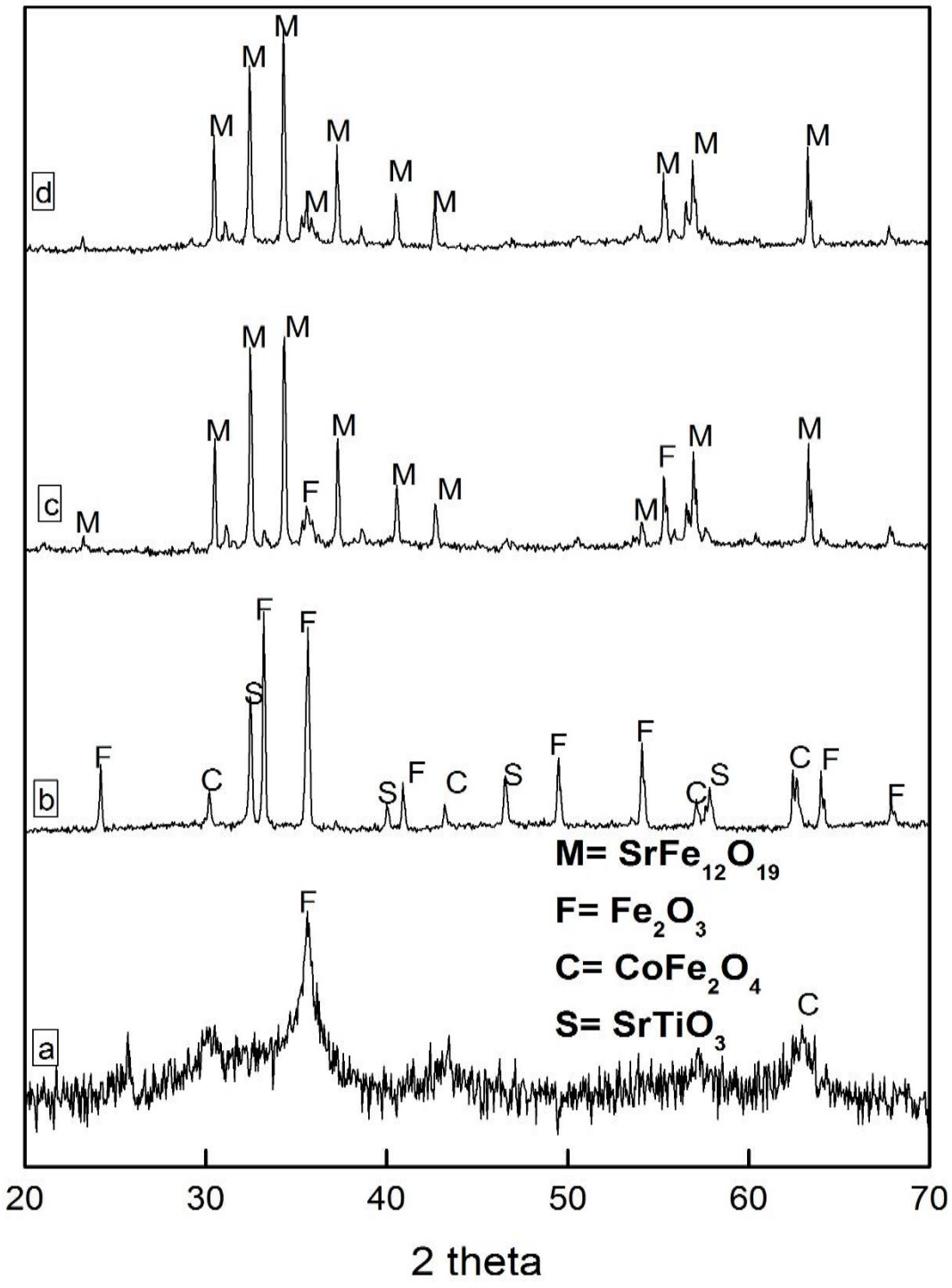

Fig. 6 Room temperature XRD pattern of Sr-M hexaferrite precursor powder calcined at (a) as burnt, (b)1000 (c) 1100 and (d) 1200°C. Major phases identified are also shown in the figure.

The as-combusted powder shows no peaks for TiO_2 (Fig 6a) but it shows peaks of iron oxide and cobalt iron oxide because some amount of iron oxide and cobalt ferrite crystallized during the combustion. The as burnt powder was directly calcined at 1000°C. Fig 6b shows the XRD pattern for that powder. It contains Fe_2O_3 ~67%, $SrTiO_3$~17%and $CoFe_2O4$~16%.

However, when the powder was calcined at 1100°C, almost 87% Sr-M (Fig 6c) phase formation occurred. Remaining phase was iron oxide ~13%. Finally 100% Sr-M phase was formed after calcining at 1200°C (Fig 6d).

Lattice Parameter Calculation

The lattice parameter of Sr-M ferrite was calculated through Rietveld refinement. Fig. 7 shows the Rietveld refinement output for 1200°C calcined powder.

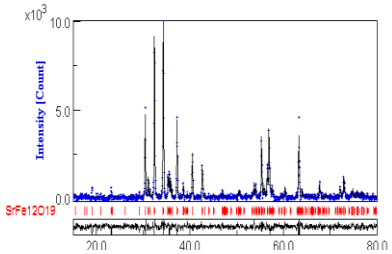

Fig.7 Rietveld output for Co-Ti-Sr-M ferrite, showing observed (+), calculated (solid line) XRD profile, their differences in the bottom and position of allowed Bragg reflections (tick marks) for two phases. Sig = 1.35, Rw= 1.60, Rb=1.18.

The lattice parameters were *a* = 5.8716 Å and *c*= 22.9580 Å. This is very similar to the standard JCPDS file 79-1411 where a= 5.8758 Å and c= 22.9580 Å. In our present compound 'c' value is higher than the standard one, because there has been the substitution of small amount of higher ionic radius Ti^{4+} ion in place of Fe^{3+}.

Dilatometry Analysis

Dilatometric curves (Fig. 8) show that the densification behavior that is the shrinkage with application of temperature. The curves are almost similar in all the compositions. Generally CuO is added in different ferrite or ferroelectric material to produce eutectic liquid composition, during sintering. However in the present case CuO reacts with hexagonal ferrite to form new compounds. That may be the reason that sintering behavior is affected in very small magnitude with addition of CuO.

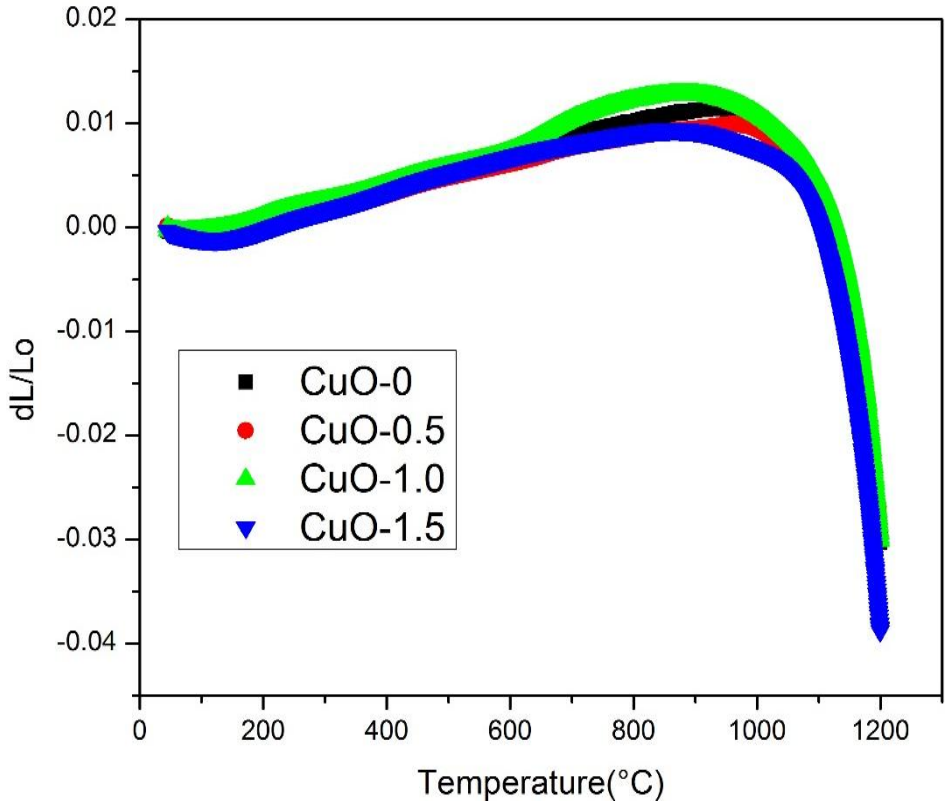

Fig.8 Dilatometry curve for different compositions.

Characterization of Sintered Pellets

Bulk Density and Apparent Porosity

With addition of CuO, bulk density normally increases and apparent porosity decreases as shown in Fig. 9. This may be due to the small effect of CuO liquid phase sintering. On set temperature of shrinkage as shown in Fig. 8 was lowest in case of 1.5% CuO composition. This indicates that CuO is helping in sintering in a limited way.

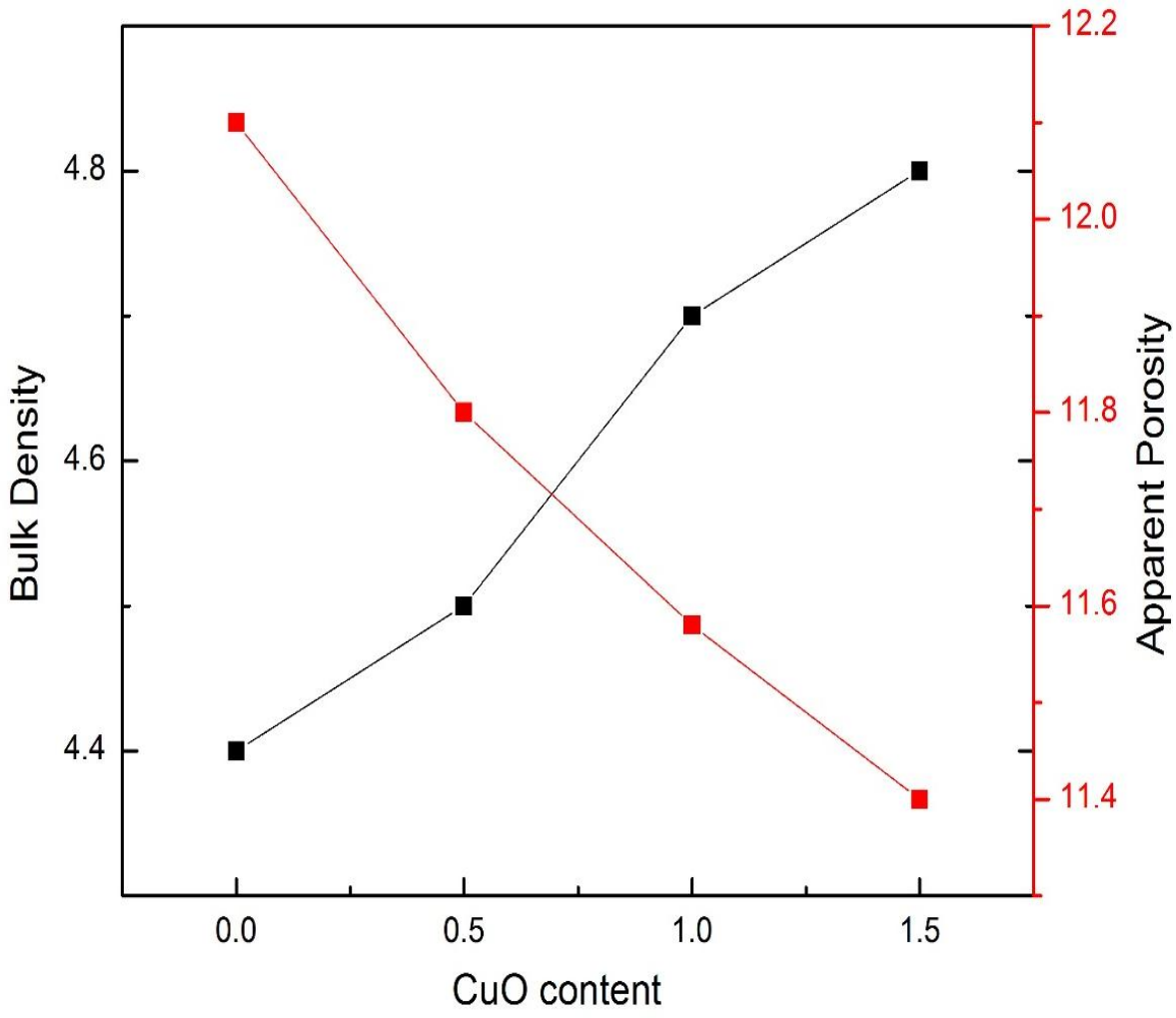

Fig. 9 Bulk density and apparent porosity variation with CuO content

Phase Evolution in Sintered Pellets

Sintered specimens were also characterized by XRD. Fig. 10 shows the XRD pattern of sintered Co-Ti substituted Sr-M hexaferrite which were doped with different amount of CuO.

Fig 10a shows pure Sr-M phase because there was no copper added to this specimen. Fig 10b shows the XRD pattern for 0.5% CuO added sintered specimen. The pattern shows presence of almost 100% hexagonal ferrite. However the peak intensities were different in some specific 2theta angle. It was difficult to explain the same. The pattern was also refined through Rietveld refinement. Fig 11 shows the Rietveld refinement output of CuO 0.0% and specimens. The CuO 0.5 % output shows some extra peaks corresponding to the formation of new compound. It has been reported that Ba-M and Sr-M pure hexagonal ferrites are stable upto the 0.5weight% of CuO. To investigate this in more detail, the XRD pattern for 1 and 1.5 weight% CuO specimens were analyzed.

Identification shows that the new compound was forming by decomposition of Sr-M hexagonal ferrite and those were mainly cubic ferrite composed of $CoFe_2O_4$ and $Cu\ Fe_2O_4$.

Also another phase is forming with an approximate composition (Sr-Ti-Fe-Cu) oxide. For example 1% CuO containing specimen was analyzed to contain about 60% cubic ferrite and 40% Sr-M hexagonal ferrite. However there was no hexagonal ferrite found in 1.5 weight% containing specimen. It may be concluded that for Co-Ti-Sr hexaferrite, CuO additives must be used in an amount less than 0.5weight% to retain hexagonal ferrite in the composition.

An interesting phenomenon may be observed from the study that the CuO additives can be used to prepare a composite having hexagonal ferrite and cubic ferrite which is evident in the case of 0.5 and 1weight % CuO containing compositions. So it opens a new avenue for research in these composite materials.

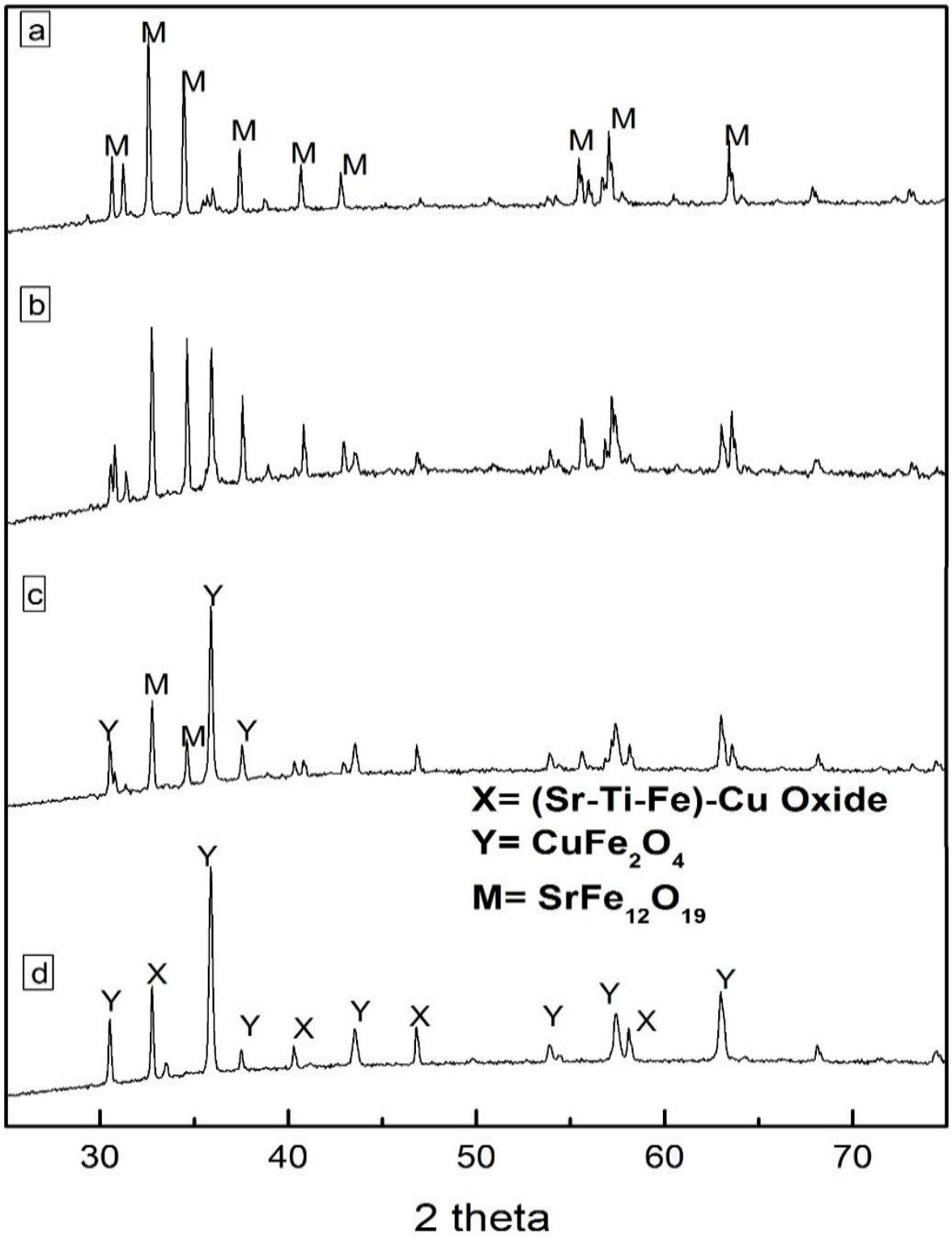

Fig.10 XRD pattern of sintered pellets with CuO (a) 0.0 (b) 0.5 (c) 1.0 and (d) 1.5 and those sineterd at 1250°C.

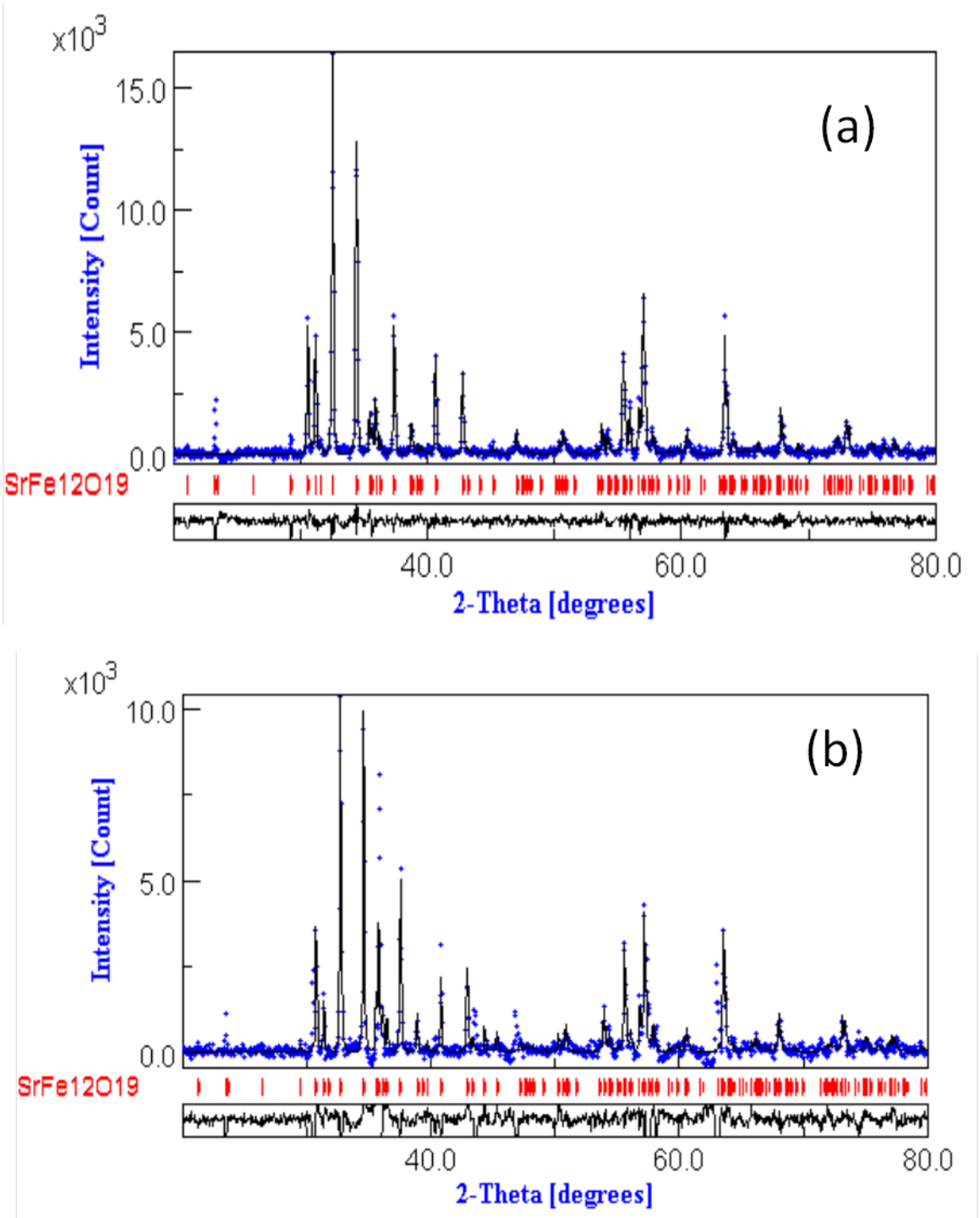

Fig. 11 Rietveld refinement plot for sintered pellet with (a) CuO-0.0 with Sig = 1.35, Rw= 1.60, Rb=1.18. Cu 0.0 sintered pellet: a=5.8719 and c= 23.05056and (b) CuO 0.5% having : a= 5.8752 and c= 23.0521 Sig=3.221, Rw= 3.372, Rb= 1.8452 , after sintered at 1250°C, showing observed (+), calculated (solid line) XRD profile, their differences in the bottom and position of allowed Bragg reflections (tick marks) for two phases.

Electrical Properties

Permittivity

The Fig. 12 shows that permittivity of specimen decreases with increase in frequency which is the typical phenomenon. It also shows that permittivity increases with increase in CuO content. This may be due to decomposition of Sr-M hexaferrites into cubic ferrite in the composition. In general the permittivity of cubic ferrite is higher than hexagonal ferrite.

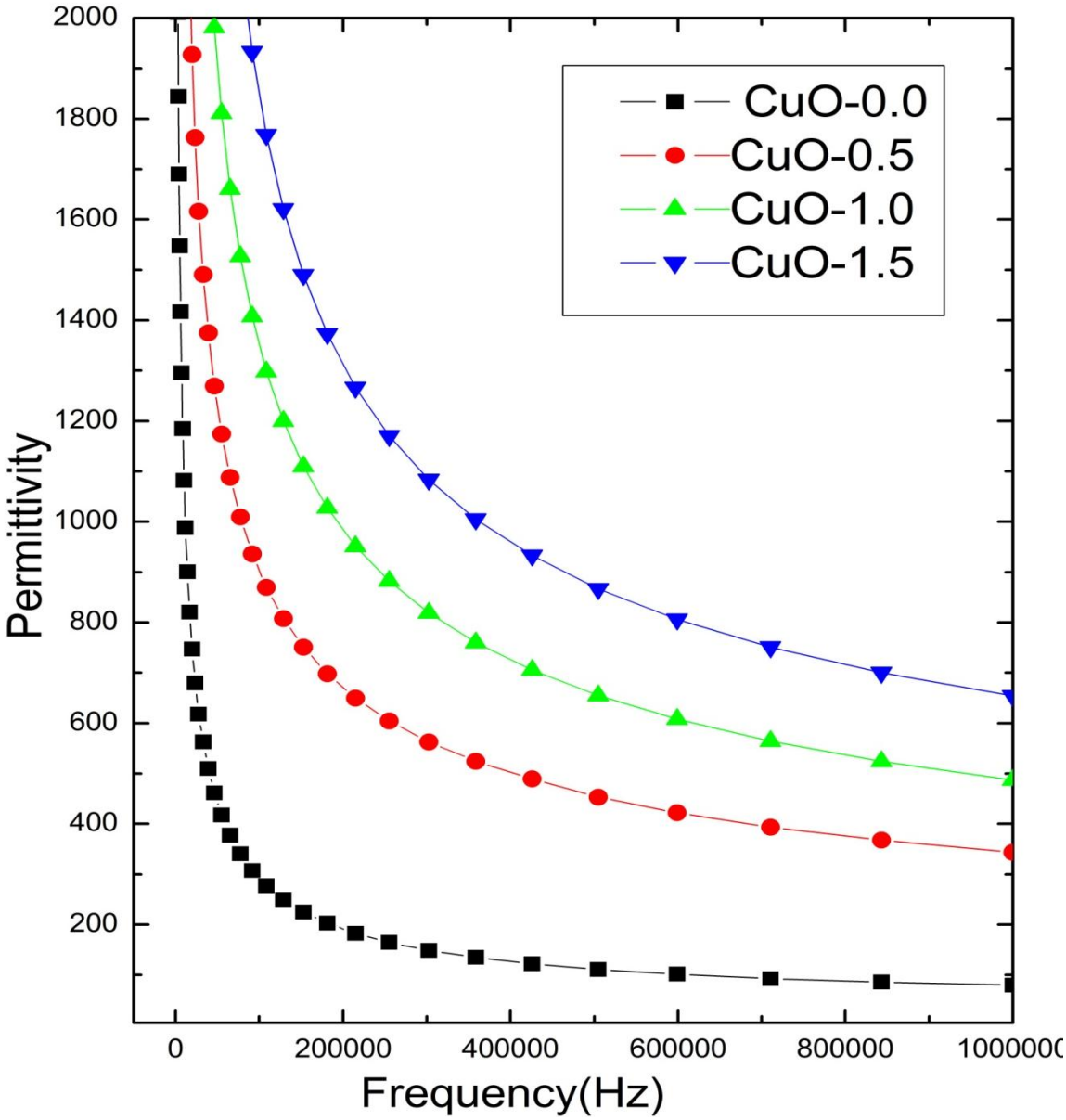

Fig. 12 Frequency dependency of initial permeability in ferrites with different CuO content.

Resistivity

Fig. 13 shows that resistivity decreases with increase in CuO which indicates that undoped specimen has highest resistivity. With addition of CuO, hexagonal ferrites start decomposing. The decomposed products remain in the grain boundary region. That may be the one reason for decrease in resistivity with increase in CuO content.

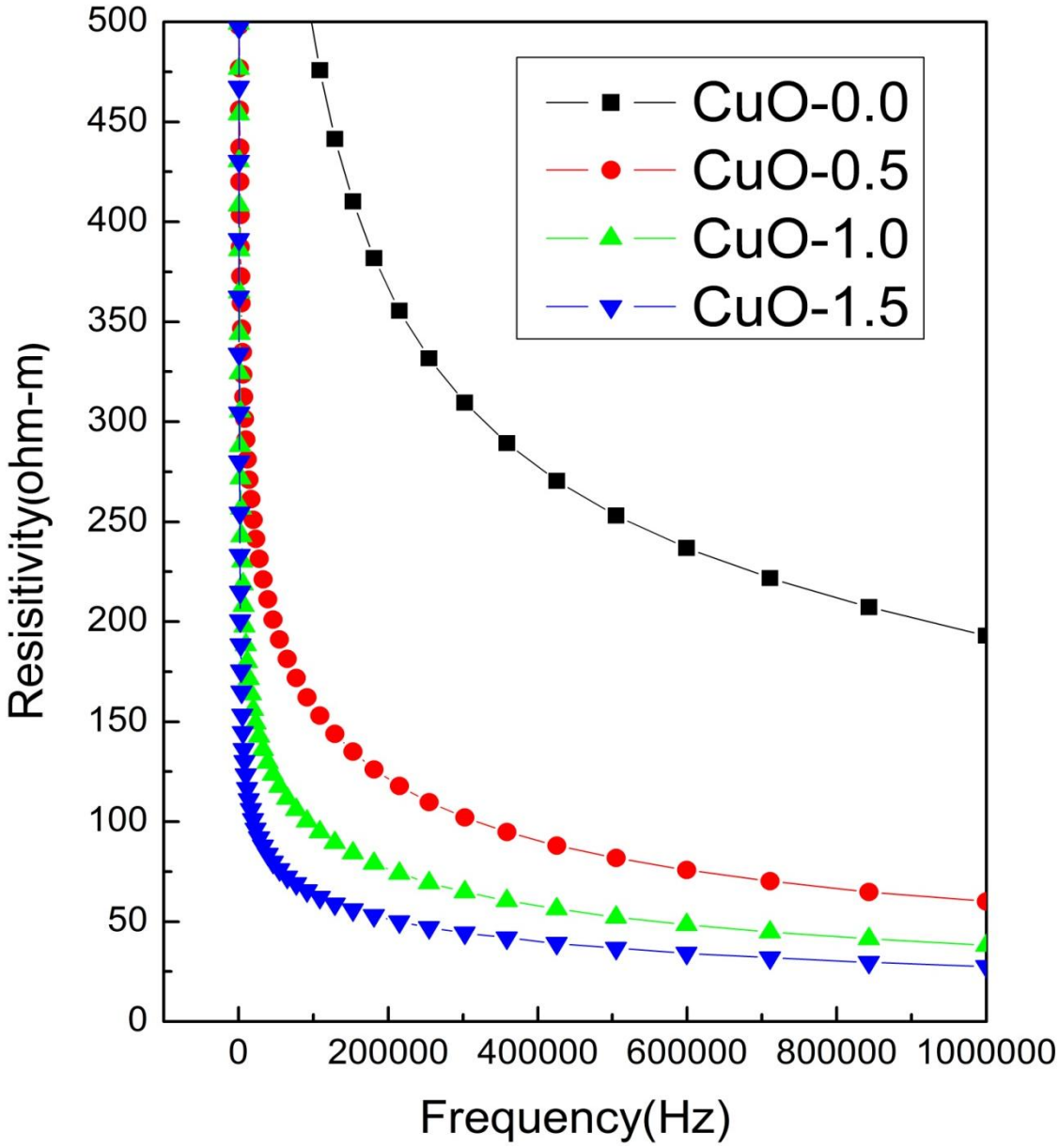

Fig. 13. AC resistivity as a function of frequency in ferrite pellets with different CuO content.

Dielectric Loss

Fig. 14 shows the variation of dielectric loss with frequency. It shows that dielectric loss decreases with increase in frequency at higher frequency. Also addition of CuO results in increase of dielectric loss as the addition level is increased because resistivity of the samples decreased with increase in CuO content.

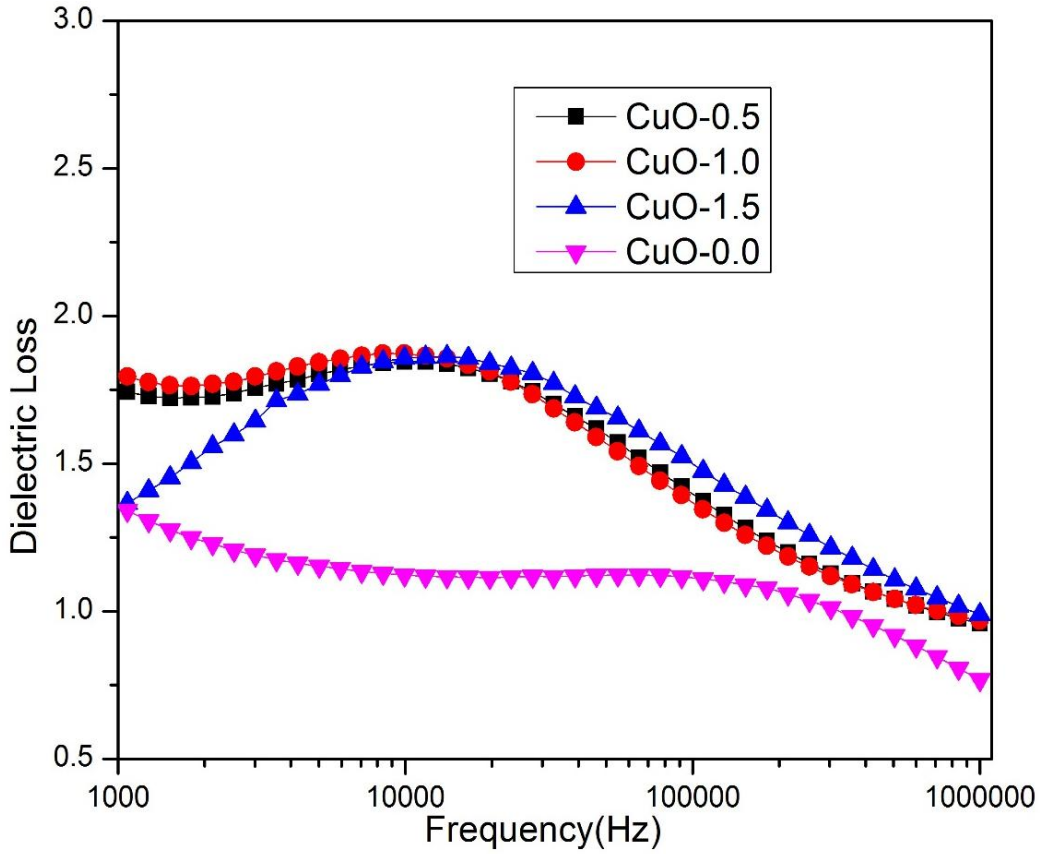

Fig.14. Dielectric loss of pellets with frequency

Magnetic Properties

Initial Permeability

Fig. 15 shows the variation of initial permeability with frequency. Initial permeability decreases with increase in frequency because the switching of magnetic domains is restricted

by domainn walls and so their response decreases significantly at higher frequencies. With increase in CuO content, initial permeability at higher frequencies increases and this happens due to decomposition of hexagonal ferrites into cubic ferrites.

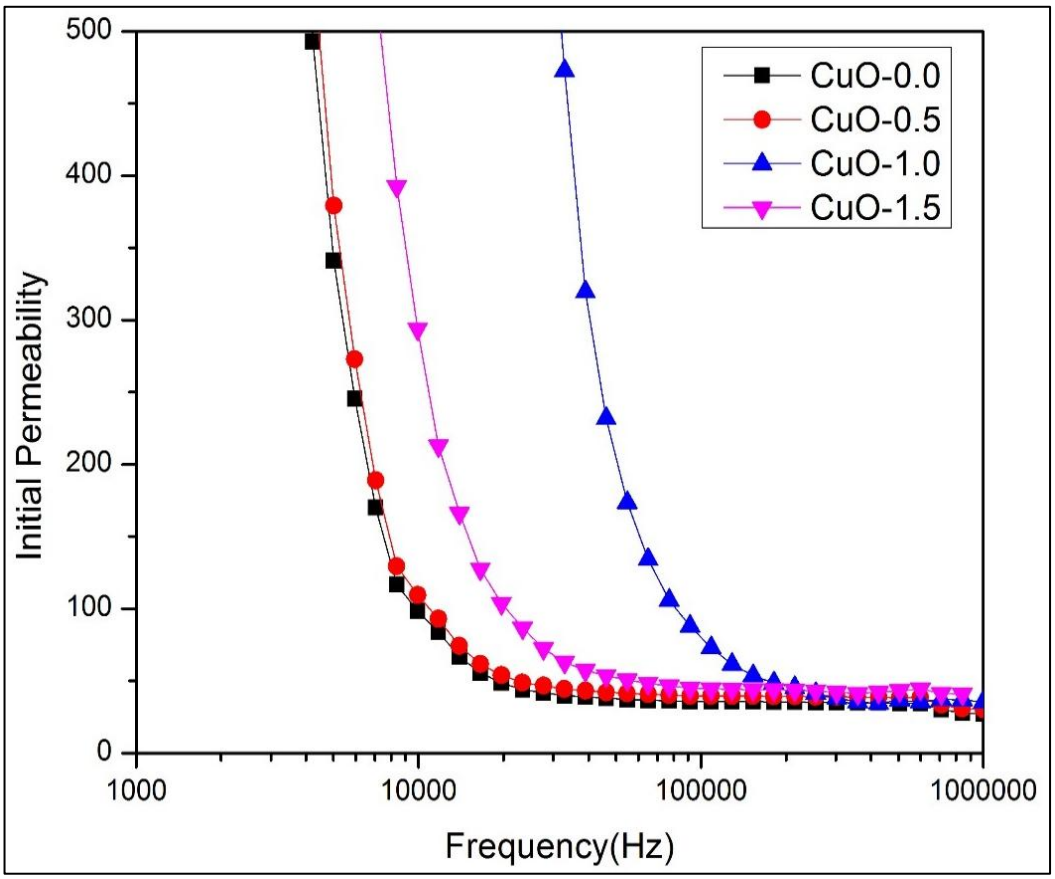

Fig. 15. Dependence of initial permeability on frequency for torroids with different amount of CuO

Relative Loss Factor

The ratio of magnetic loss (tan δ) to initial permeability (μ') is also known as Relative Loss Factor (RLF). RLF is an important parameter for the inductors to be used at higher frequency and a low RLF is desirable. Fig. 16 shows the variation of relative loss factor with frequency.

RLF decreases with increasing frequency and also with increasing amount of CuO in the composition. The composition having Cu)-1.5 weight % has lowest RLF.

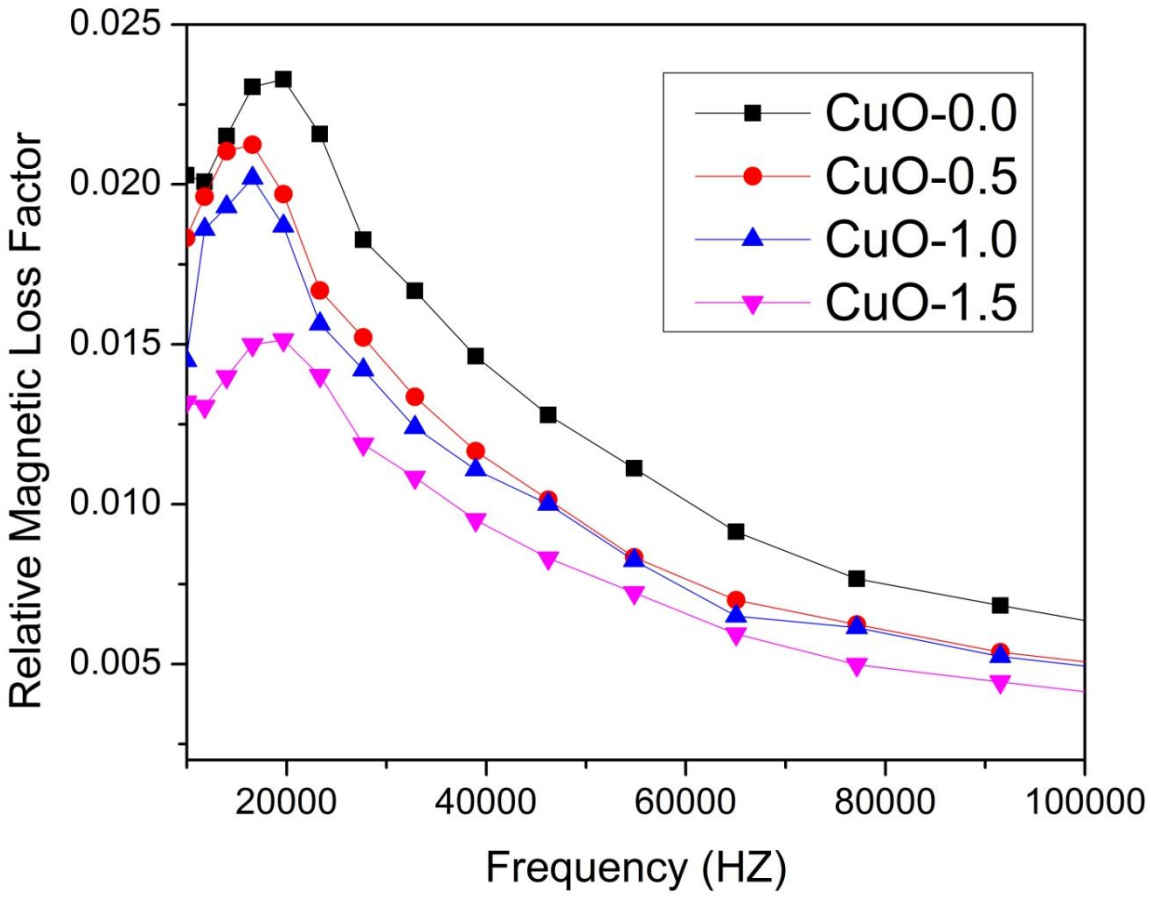

Fig.16. Variation of relative loss factor for torroids of different compositions with frequency

Microstructural Analysis

SEM microstructues shows that average grain size of CuO containing sample is around 5µm. Fig 17 shows that upon CuO addition grain size increases. Also there is change in grain shapes

which is prominent in the samples containing CuO-1.0 and CuO-1.5, The highest grain size was observed in in CuO-1.5 specimen which also supports the bulk density data. Bulk density of CuO-1.5 was highest among all. Also CuO-1.5 specimen is very compact. The change in shape may be due to the growth of cobalt ferrite from the hexagonal matrix.

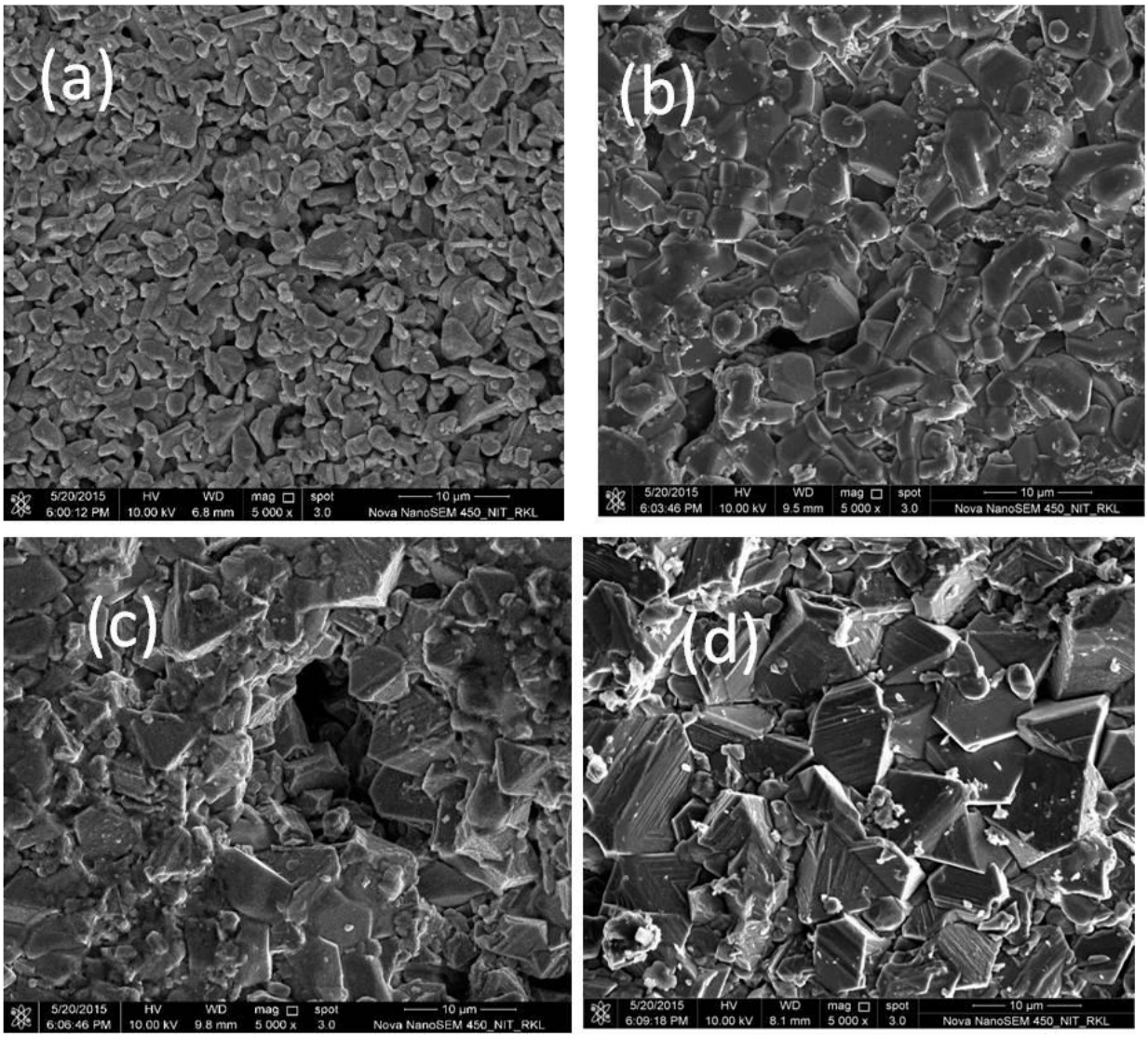

Fig.17 SEM micrograph of (a) CuO-0. (b) CuO-0.5 (c) CuO-1.0 (d) CuO-1.5 ceramics

Chapter 5

Conclusion

Conclusion

Effect of CuO addition on the hexagoal ferrite ($SrCo_{1.3}Ti_{1.3}Fe_{9.4}O_{12-\delta}$) has been investigated. (Co-Ti-Sr)- M hexaferrite compositions were synthesized by sol-gel auto combustion method. Pure ferrite phase was achieved after cacination at 1200°C. However the addition of copper oxide resulted in decomposition of hexagonal ferrite phase into $CoFe_2O_4$ phase.

In case of 1.5 weight % CuO added specimen, the material was composed of cobalt ferrite and CuO based phases. Densification study shows that bulk density increases with increase of CuO as well as grain size also increases.

Permittivity of the ferrites increases with increase in CuO addition and it was highest in 1.5 weight% CuO containing sample. This is due to formation of cubic ferrite phase.

Chapter 6

REFERENCES

Refereances

[1] Smit J, Wijn HPJ. Ferrites, Philips Technical Library, Eindhoven; 1959.

[2] Robert C. Pullar, Progress in Materials Science 57 (2012) 1191–1334

[3] J. Mürbe, J. Töpfer, Journal of the European Ceramic Society 32 (2012) 1091–1098

[4] Nobuyoshi Koga, TakanoriTsutaoka, Journal of Mag and Mag Mate. 313 (2007) 168–175

[5] United States Patent Application Pub. No.: US 2012/0085963 A1, Apr.12, 2012.

[6] http://www.tdk.co.jp/techjournal_e/vol04_mlg/contents04.htm

[7] SilviaBierlich, JörgTöpfer, IEEE Transactions On Magnetics, Vol. 48, No. 4, 2012

[8] T. Tachibana, T. Nakagawa, Y. Takada, T. Shimada, and T. Yamamoto, J. Magn. Magn.Mater.vol. 284, pp. 369–375, 2004.

[9] Y. Bai, J. Zhou, Z. Gui, and L. Li, J. Magn. Magn. Mater., vol. 246, pp. 140–144, 2002.

[10] S. Bierlich,J.T¨opfer, J. Magn. Magn. Mater, 324 (2012) 1804–1808

[11] S. Krauunovská and J. Töpfer, J. Magn. Magn. Mater, vol. 320, pp. 1370–1376, 2008.

[12] Narang SB, Huidara LS. J Ceram Process Res 2006;7:113.

[13] Yamamoto H, Kumehara H, Takeuchi R, Nishio N. J Phys IV 1997;7:C1–535.

[14] Pullar RC, Taylor MD, Bhattacharya AK. J Mater Res 2001;16:3162.

[15] Jean M, Nachbaur V, Bran J, Le Breton J-M. J Alloys Compd 2010; 496:306.

[16] Sato H, Umeda T. In: Ferrites, proc ICF6, Kyoto and Tokyo; 1992. p.1122.

[17] Zhong W, Ding W, Jiang Y, Zhang N, Zhang J, Du Y, et al. J Am Ceram Soc 1997;80:3258.

[18] R. Lebourgeois, “Ferrite Material for a Permanent Magnet and Method for Production”; Patent: WO 2004/102595, PCT/EP2004/050825, May 17th 2004.

[19] DarjaLisjak and Richard Lebourgeois, J. Am. Ceram. Soc., 95 [10] 3025–3030 (2012)

[20] WandeeOnreabroy ,KomanePapato , GobwuteRujijanagul ,KamonpanPengpat , TaweeTunkasiri.Ceramics International 38S (2012) S415–S419

[21] Ali Ghasemi, Vladimir ˇSepela´k,Journal of Magnetism and Magnetic Materials 323 (2011) 1727–1733

[22] Qingqing Fang, Yanmei Liu, Ping Yin, Xiaoguang Li. Journal of Magnetism and Magnetic Materials 234 (2001) 366–370

[23] Xiansong Liu, Pablo Herna´ndez-Go´ mez, Kai Huang, Shengqiang Zhou,Yong Wang, Xia Cai, Hongjun Sun, Bao Ma. Journal of Magnetism and Magnetic Materials 305 (2006) 524–528

[24] Ali Ghasemi. Journal of Magnetism and Magnetic Materials 324 (2012) 1375–1380

[25] Kubo et. al. US patent No. 5378547

[26] Z.Yue, L. Li,J. Zhou,H. Zhang,Z. Gui, Mat. Sci. Engg. B 64 (1999) 68.

[27] M. D. Nersesyan, A. G. Peresada, A.G. Merzhanov, Int. J. SHS 7 (1998) 60.

[28] S. R. Jain, K. C. Adiga, Combustion and Flame 40 (1981)71.